# Further insight into the tunneling contribution to the vibrational relaxation of NO in Ar

E. I. Dashevskaya, I. Litvin, E. E. Nikitin, and J. Troe

Citation: The Journal of Chemical Physics **142**, 164310 (2015); doi: 10.1063/1.4919126
View online: http://dx.doi.org/10.1063/1.4919126
View Table of Contents: http://scitation.aip.org/content/aip/journal/jcp/142/16?ver=pdfcov
Published by the AIP Publishing

# Further insight into the tunneling contribution to the vibrational relaxation of NO in Ar

E. I. Dashevskaya,[1,2] I. Litvin,[3] E. E. Nikitin,[1,2] and J. Troe[2,3,a)]
[1]*Schulich Faculty of Chemistry, Technion—Israel Institute of Technology, Haifa 32000, Israel*
[2]*Max-Planck-Institut für Biophysikalische Chemie, Am Fassberg 11, D-37077 Göttingen, Germany*
[3]*Institut für Physikalische Chemie, Universität Göttingen, Tammannstrasse 6, D-37077 Göttingen, Germany*

(Received 23 February 2015; accepted 16 April 2015; published online 29 April 2015)

Tunneling corrections to Landau-Zener rate coefficients for the vibrational relaxation NO($X^2\Pi, v = 1$) + Ar → NO($X^2\Pi, v = 0$) + Ar between 300 and 2000 K are determined employing *ab initio* potential energy surfaces calculated by the code provided by Alexander [J. Chem. Phys. **111**, 7426 (1999)]. The calculations use a reaction coordinate approach and lead to vibronically nonadiabatic transition probabilities within the generalized Airy approximation as extended to the WKB under-barrier Landau-Lifshitz limit. The calculations confirm experimental evidence for an onset of major tunneling contributions to the relaxation rate at temperatures below about 900 K and rationalize large tunneling contributions at 300 K. These effects increase the rate coefficients by several orders of magnitude over the uncorrected Landau-Zener values and remove the large gap between the latter and experimental results. © *2015 AIP Publishing LLC.* [http://dx.doi.org/10.1063/1.4919126]

## I. INTRODUCTION

The vibrational relaxation of NO demonstrates a variety of interesting features of collisional energy transfer. When the collider is a reactive atom like O, Cl, or I,[1–5] the collision complexes correspond to vibrationally highly excited polyatomic molecules above their dissociation limits, and the large efficiency of energy transfer is governed by intramolecular energy redistribution. The efficiency of energy transfer then can be represented by statistical unimolecular rate theory[6] and/or quantum scattering and classical trajectory calculations.[7] When the collider is polyatomic with open electronic shell like NO or $NO_2$, the situation may be similar, but resonance phenomena of V-V transfer may also be observed.[8,9] As before, the potential energy surface (PES) of the forming quasi-bound collision complexes is of central importance.[10] When the collider finally is an inert rare gas atom, vibrational energy transfer still may be far more efficient than estimated on the basis of the Landau-Teller (LT) mechanism (transitions between vibrational states supported by uncoupled Born-Oppenheimer (BO) PESs as described in the original LT approach,[11] the Schwartz-Slawsky-Herzfeld (SSH)[12] treatment, or its semiclassical generalization[13]). The reason for this enhancement of efficiency may again be found in the open-electronic shell character of NO. However, it is quite different from the situation of NO–NO collisions.[10] Instead, the NO-rare gas interaction may give rise to crossing of rovibronic PESs, which influences the vibrational relaxation rates,[14–16] through the Landau-Zener (LZ) mechanism (transitions between vibronic states, i.e., vibrational states supported by nonadiabatically coupled BO PESs). In a recent publication,[17] we have treated the vibrational relaxation

$$\mathrm{NO}(X^2\Pi, v = 1) + \mathrm{Ar} \rightarrow \mathrm{NO}(X^2\Pi, v = 0) + \mathrm{Ar} \qquad (1.1)$$

by such a vibronic curve crossing mechanism and, in this way, suggested a rationalization of experimental data at room temperature from Refs. 18 and 19 and in the range 900–1500 K from Refs. 1 and 20. Although there are still discussions about the accuracy of the room temperature data,[9] there appears only little doubt about the large efficiency of process (1.1) at low temperatures.

By an extension of the LZ curve-crossing approach to include tunneling expressed by Airy functions (see the Landau-Lifshitz, LL,[21] approximation), in our previous work,[17] the experimental data could be reconciled with a minimum number of adjustable parameters, the most relevant being the minimum crossing energy of the highest PES originating from $v = 0$ and the lowest PES originating from $v = 1$ within the multitude of NO–Ar vibronic potentials. In this way, we have calculated tunneling correction factors $C(T)$ to the standard Landau-Zener rate coefficient ${}^{\mathrm{LZ}}k_{10}(T)$ using the Airy approximation to the nonadiabatic transition probabilities and approximately extending it to the WKB Landau-Lifshitz limit for nonlinear diabatic potentials. At the present stage, a full quantum scattering approach with a multi-dimensional tunneling does neither appear feasible nor appropriate. For this reason, we restrict ourselves to a one-dimensional model with a suitable reaction coordinate and the corresponding one-dimensional tunneling contribution.

In our previous work,[17] the reaction coordinate and the dividing surface for the crossing multi-dimensional PESs were found from an asymptotic description of the spacing between the relevant vibronic PESs. The latter was assumed to be governed by the exchange interaction between the electrons of the Ar atom and an unpaired $2\pi'$ electron of NO.[15,16] By using interaction parameters from the asymptotic theory, we predicted the temperature dependence of $C(T)$ for a reasonable

a)Email: jtroe@mpibpc.mpg.de

 

range of other parameters that are also of relevance for the treatment. In the present article, we go one step further. Here, we present calculations of $C(T)$ with two improvements. First, the fitting of parameters is replaced by the direct use of *ab initio* PESs for the NO–Ar interaction from Alexander.[22] Second, the nonadiabatic probabilities are calculated in a generalized Airy (GAi) approximation which interpolates between LZ- (classically allowed collision energies) and LL- (classically forbidden collision energies) WKB limits through the non-WKB energy range in the vicinity of the crossing point energy $E_a$ where the probability is expressed through the Airy function.[21] The main objective of the present work, thus, is the extrapolation of high-temperature rate coefficients, where tunneling is not important, to lower temperatures where the tunneling is expected to be dominant. By the use of the *ab initio* PESs, this treatment intends to avoid the necessity to employ parameter fitting in the calculation of the tunneling correction to the high-temperature rate coefficient.

The plan of the article is the following. In Sec. II, we describe the relevant vibronic *ab initio* PESs and define a reaction coordinate as well as a dividing surface. Furthermore, the diabatic potentials along the reaction coordinate are illustrated. In Sec. III, we consider the generalized Airy approximation and use it for the calculation of the nonadiabatic tunneling probabilities as a function of the energy along the reaction coordinate. In Sec. IV, tunneling correction factors $C(T)$ to ${}^{\mathrm{LZ}}k_{10}(T)$ are derived from these probabilities. Sec. V compares theory and experiment, and Sec. VI concludes the article.

## II. DIABATIC POTENTIAL ENERGY SURFACES

Neglecting spin-orbit coupling, the BO PESs of the NO–Ar system depend on three coordinates, the internuclear distance $r$ in NO, the distance $R$ between the center-of mass of NO and Ar, and the angle $\theta$ between the vectors $\mathbf{r}$ and $\mathbf{R}$ with $\theta = 0$ corresponding to the linear Ar–NO arrangement. The two BO PESs that correlate with separated NO($X^2\Pi$) and Ar($^1S_0$) differ in their reflection symmetry with respect to the plane of the system ($U'(r,R,\theta)$ for symmetric $A'$ and $U''(r,R,\theta)$ for anti-symmetric $A''$ states). Since details of the weak nonadiabatic coupling between $A'$ and $A''$ states are not discussed here, we concentrate on the considered BO PESs. Upon using an adiabatic approximation with respect to the perturbed vibrational motion of NO, a set of vibronic PESs, $W'_{v_s}(R,\theta)$ and $W''_{v_a}(R,\theta)$, is generated. The following discussion will be centered on those two states which correlate with the vibrational states $v = 0$ and $v = 1$ of free NO and which exhibit a crossing, namely, $|A', v_s = 0\rangle$ and $|A'', v_a = 1\rangle$. The curve-crossing mechanism of the vibrational relaxation of NO relates the change in the vibrational quantum number of NO upon collision with Ar with the nonadiabatic coupling between the two states induced by the relative motion of NO and Ar, by the vibration of NO, as well as by spin-orbit and Coriolis interaction.[14] This coupling is the strongest near the crossing line (CL) $R = R_c(\theta)$ which is defined by the condition

$$W'_0(R,\theta) = W''_1(R,\theta). \tag{2.1}$$

Vibrationally adiabatic PESs differ from their counterparts calculated for fixed internuclear distance of NO. However, for low vibrational states, the difference in the interaction energy between the vibrationally adiabatic and fixed-nuclei (with $r = r_e$) approximations will only be of the order of the ratio $E_{vib}/D$, where $E_{vib}$ is the vibrational energy of the diatomic and $D$ is its dissociation energy.[23] For $v = 0$ and $v = 1$, the ratio $E_{vib}/D$ does not exceed a few percent, and this characterizes the accuracy of the fixed-nuclei approximation in the calculation of the interaction.

Within the described approximation, $W'_1(R,\theta)$ and $W''_0(R,\theta)$ are expressed through the *ab initio* potentials $V'(R,\theta)$ and $V''(R,\theta)$ as calculated and discussed in Ref. 22. In this reference, the average potential $(1/2)(V'' + V')$ and the half difference $(1/2)(V'' - V')$ are expressed in the form of expansions in $\theta$-dependent Legendre polynomials and Wigner $d$-functions. For $R > 5.2$ a.u. and within a limited energy range, the $R$-dependent expansion coefficients are shown in Figs. 1 and 2 of Ref. 24. For shorter distances, we have calculated the expansion coefficients by the numerical code supplied to us by Alexander.

The potentials $V'(R,\theta)$ and $V''(R,\theta)$ define the initial PES ($V_i(R,\theta)$, for approaching collision partners NO($X^2\Pi, v = 1$) + Ar), and the final PES ($V_f(R,\theta)$, for receding collision partners NO($X^2\Pi, v = 0$) + Ar). They are expressed as

$$\begin{aligned} V_f(R,\theta) &= V'(R,\theta) - \Delta E_{10}, \\ V_i(R,\theta) &= V''(R,\theta), \end{aligned} \tag{2.2}$$

where $\Delta E_{10}$ is the asymptotic energy difference between two vibronic states. In this approximation, the CL $R = R_c(\theta)$ is defined as the solution of the equation

$$V_i(R,\theta) = V_f(R,\theta). \tag{2.3}$$

The PES of $V_i(R,\theta)$ has a simpler structure than that of $V_f(R,\theta)$: it is qualitatively similar to the PES of a $N_2$–Ar system since the exchange interaction of the electrons of the Ar atom with the electron of the $2\pi''$ MO of NO is very weak because the nodal plane of this orbital coincides with the plane of system. The difference potential $\Delta V(R,\theta) = V' - V''$, in contrast to this, is dominated by the exchange interaction of the electrons of the Ar atom with the electron of the $2\pi'$ MO of NO.[15–17] The potential $V_i(R,\theta)$ along the CL possesses two minima, $E_a$ and $E'_a$, located in the first $(0 < \theta < \pi/2)$ and the second $(\pi/2 < \theta < \pi)$ quadrants of the $R,\theta$-plane. The latter energy ($E'_a/k_B$ of about 29 000 K) is much higher than the former ($E_a/k_B = 5250$ K) such that it is ignored for the energy and temperature range discussed in the present work. The former energy corresponds to the configuration $\theta = \theta_a$ and $R_a = R_c(\theta_a)$, and it is used later on as defined by

$$E_a = \min\{V_i(R,\theta)\}|_{R=R_c(\theta)} = V_i(R_a,\theta_a). \tag{2.4}$$

For the reasons outlined before, in the following, we will consider only the first quadrant of the Cartesian frame ($x = R\cos\theta$, $y = R\sin\theta$). In the reaction-coordinate approach, one employs a one-dimensional model with motion along the reaction coordinate $z$ which is chosen perpendicular to the CL at the point $(R_a,\theta_a)$ and which has a slope $k = \tan\theta_q$ in the $(x,y)$ frame. The information needed for the calculation of nonadiabatic transition probabilities is contained in the intersections of the potentials $V_i = V''(R,\theta)$ and $V_f(R,\theta)$ along the reaction coordinate $z$. Since the range of $z$, which contributes to the

probability, is expected to be small compared to the extension of the PESs, which is related to the anisotropy of the interaction (i.e., the condition for the local separation of variables), the variation of $R$ and $\theta$ along $z$ can be represented by linear functions of $z$,

$$\begin{aligned} R &= R_a + z\cos\Delta\theta_{qa}, \\ \theta &= \theta_a + (z/R_a)\,\sin\Delta\theta_{qa}. \end{aligned} \tag{2.5}$$

Here, $\Delta\theta_{qa} = \theta_q - \theta_a$ is the angle between the vector **R** from the NO center of mass to the Ar atom and the reaction coordinate at the crossing point. The forces $F_{i,f}$ along the reaction coordinate at the crossing point are

$$\begin{aligned} F_{i,f} = &-\left(\partial V_{i,f}(R,\theta)/\partial R\right)\big|_{R=R_a,\theta=\theta_a}\cos\Delta\theta_{qa} \\ &-\left(\partial V_{i,f}(R,\theta)/R\partial\theta\right)\big|_{R=R_a,\theta=\theta_a}\sin\Delta\theta_{qa}. \end{aligned} \tag{2.6}$$

The initial and final PESs, $V_i(R,\theta)$ (red solid lines) and $V_f(R,\theta)$ (magenta solid lines), are illustrated in Fig. 1 through equipotential lines (to the left and to the right of the reaction coordinate, the latter represented by the green straight line). The solid blue line corresponds to the CL. Note that the spacing between the equipotential lines for $V_f(R,\theta)$ is smaller than for $V_i(R,\theta)$ since the former is more repulsive than the latter. The circle corresponds to the minimum energy along the crossing line.

In the following, we use scaled values of the reaction coordinate, $\zeta = z/a$ with $a$ being an appropriate length, and scaled values of the potential energy, $\upsilon_{i,f} = V_{i,f}/E_a$. We then have

$$\begin{aligned} \upsilon_i(\zeta) &= \left(V_i(R,\theta)/E_a\right)\big|_{R=R(\zeta),\theta=\theta(\zeta)}, \\ \upsilon_f(\zeta) &= \left(V_f(R,\theta)/E_a\right)\big|_{R=R(\zeta),\theta=\theta(\zeta)}. \end{aligned} \tag{2.7}$$

The length $a$ is defined by the condition that the scaled force (the negative derivative of the scaled potential with respect to the scaled reaction coordinate) for the initial PES, $\varphi_i$, is equal to unity. Then, the scaled force for the final PES can be written as $1+\delta$. This implies

$$\varphi_i = F_i a/E_a = 1, \quad \varphi_f = F_f a/E_a = 1+\delta. \tag{2.8}$$

The two expressions of Eq. (2.8) define $a$ and $\delta$. The scaled potentials of Eq. (2.7), with the functions $R(\zeta)$ and $\theta(\zeta)$ from Eq. (2.5), are shown in Fig. 2 over the energy range $0.25 < \upsilon_i,\ \upsilon_f < 2$ (red and blue lines).

The essential parameters of the two considered *ab initio* PESs are listed in Table I. Also given is the derivative $dR_c(\theta)/d\theta|_{\theta=\theta_a}$ that characterizes the anisotropy and enters into the expression for the effective mass (see Sec. III).

The inverse scaling length, found from the slope of the potential $\upsilon_i$ that converges asymptotically to zero, is close to the value of $2a_0^{-1}$ as expected for the radial dependence of the exchange interaction within the asymptotic theory.[13] The difference between $2.35\,a_0^{-1}$ and $2\,a_0^{-1}$ can be ascribed to the fact that the slope of the potentials along the reaction coordinate is slightly larger than along the radial coordinate. The slope $\varphi_f$ of $\upsilon_f$ is noticeably larger than $\varphi_i$. This is the consequence of the fact that $\upsilon_i$ converges to the negative value of $-\Delta E_{10}/E_a$. These features have been simulated in Ref. 17 within a parameterized exponential model. In the present work, it was possible to relate the corresponding parameters to the properties of the *ab initio* PESs from Ref. 22.

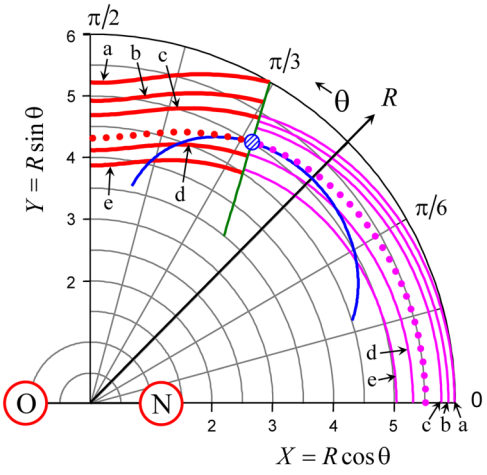


FIG. 1. *Ab initio* PESs of the NO–Ar system (red solid lines for $V_i(R,\theta)$ of NO($v=1$)+Ar and magenta solid lines for $V_f(R,\theta)$ of NO($v=0$)+Ar) with the crossing line of the potentials (blue solid line) and the reaction coordinate (green solid line). (The dotted red line corresponds to the energy $E_a/k_B = 5250$ K, which touches the crossing line at $R = R_a = 5.02\,a_0$ and $\theta = \theta_a = 0.321\,\pi$; the PES to the left of the reaction coordinate line corresponds to $V_i(R,\theta)$, the one to the right to $V_f(R,\theta)$; contour lines are given in K for $V_i(R,\theta)/k_B$ and $V_f(R,\theta)/k_B$ and correspond to 400 K (a), 1000 K (b), 2000 K (c), $E_a/k_B = 5250$ K, 10 000 K (d), and 20 000 K (e).).

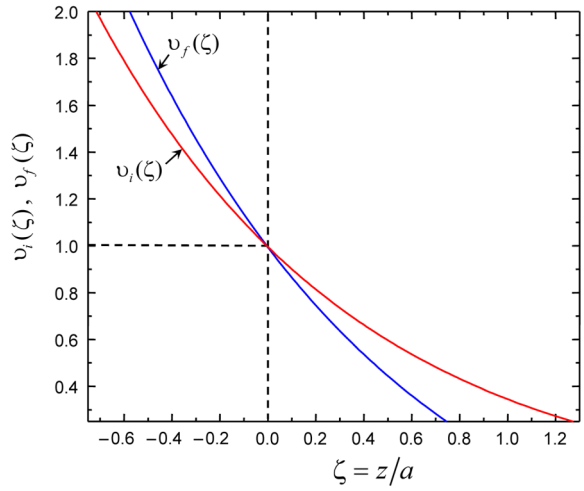


FIG. 2. Scaled *ab initio* diabatic potentials $\upsilon_i(\zeta)$, $\upsilon_f(\zeta)$ vs the reaction coordinate $\zeta = z/a$, $a = a_0/2.35$ (the range of $\varepsilon$ corresponds to $0.25 < \varepsilon < 2$ including the optimal energy $\varepsilon^*$ (see Fig. 6)).

## III. NONADIABATIC TUNNELING PROBABILITIES

In this section, nonadiabatic tunneling probabilities $P$ for the motion along the reaction coordinate are calculated within a GAi approximation. This approximation interpolates transition probabilities, $P_{GAi}$, between the classically allowed WKB range (expressed by the LZ equation) and the classically forbidden WKB range (expressed by the LL equation) through the non-WKB region in which the transition probabilities are expressed through the Airy function for linear crossing diabatic curves. Within this approach, $P_{GAi}$ depends on the difference

TABLE I. Parameters for the NO–Ar interaction as derived from the *ab initio* PES of Ref. 22 ($a_0 = 1$ a.u. $= 0.529$ Å).

| $R_a$ | $\theta_a$ | $E_a/k_B$, $\Delta E_{10}/k_B$ (K) | $dR_c(\theta)/d\theta\|_{\theta=\theta_a}$ | $\Delta\theta_{qa}$ | $a, \delta$ | $\varphi_i, \varphi_f$ |
|---|---|---|---|---|---|---|
| $5.02\,a_0$ | $0.321\,\pi$ | 5250, 2700 | $-1.30\,a_0$ | $0.0807\,\pi$ | $a = a_0/2.35, \delta = 0.357$ | $1, 1+\delta$ |

between the action integrals $S$, as calculated for the potentials $\upsilon_i$, $\upsilon_f$, and their linear (L) counterparts $S_L$, as characterized by the slopes of the potentials at the crossing point $\varphi_i = 1$, $\varphi_f = 1 + \delta$.

For classically allowed and classically forbidden energy ranges ($S^>$ and $S^<$, respectively), the expressions for the action integrals in terms of the scaled potentials of Eq. (2.7) and for the scaled energies $\varepsilon = E/E_a$ (with $\varepsilon$ counted from the asymptote of the upper PES, $\upsilon_i$), for $\varepsilon \geq 1$, are

$$S^>(\varepsilon) = w\sigma^>(\varepsilon),$$

with

$$\sigma^>(\varepsilon) = \int_{\zeta_i^>}^{0} \sqrt{\varepsilon - \upsilon_i(\zeta)}d\zeta - \int_{\zeta_f^>}^{0} \sqrt{\varepsilon - \upsilon_f(\zeta)}d\zeta \quad (3.1a)$$

and, for $\varepsilon \leq 1$, are

$$S^<(\varepsilon) = w\sigma^<(\varepsilon),$$

with

$$\sigma^<(\varepsilon) = \int_{0}^{\zeta_i^<} \sqrt{\upsilon_i(\zeta) - \varepsilon}d\zeta - \int_{0}^{\zeta_f^<} \sqrt{\upsilon_f(\zeta) - \varepsilon}d\zeta. \quad (3.1b)$$

Here, the $\zeta_i^>, \zeta_f^>, \zeta_i^<, \zeta_f^<$ are the $\zeta$ values at which the integrands are zero and

$$w = \sqrt{2\mu^* E_a}a/\hbar \quad (3.2)$$

corresponds to the WKB parameter with the effective mass $\mu^*$. The condition for a WKB motion in the field of the upper potential, $\upsilon_i(\zeta)$, reads

$$\sqrt{2\mu^* E}a/\hbar = w\sqrt{\varepsilon} >> 1. \quad (3.3)$$

The effective mass is governed by the interplay of radial and rotational motion along the reaction coordinate. Under the condition $(dR_c/d\theta)_{\theta=\theta_a} << R_a$, it is given by[13]

$$\mu^* = \mu/\left(1 + \mu\,(dR_c/d\theta)^2_{\theta=\theta_a}/Mr_e^2\right). \quad (3.4)$$

Here, $\mu$ denotes the reduced mass of the NO–Ar pair, $\mu = 17.14$ amu, $M$ is the reduced mass of NO, and $r_e$ is its equilibrium internuclear distance. With the value of $(dR_c/d\theta)_{\theta=\theta_a}$ from Table I and $M = 7.47$ amu, $r_e = 2.175\ a_0$, one finds $\mu^* = 0.55\mu = 9.43$ amu $= 1.72 \times 10^4\ m_e$. The difference between $\mu$ and $\mu^*$ characterizes the contribution of the hindered rotation of NO to the motion along the reaction coordinate. With the parameters of Table I, one then has $w = 10.3$. If in Eq. (3.2), one would use the reduced mass $\mu$ instead of $\mu^*$, the respective value of the WKB parameter would increase by 35%.

With linear approximations for $\upsilon_{i,f}$, the quantities $S_L^{>,<}$ and $\sigma_L^{>,<}$ are calculated from Eqs. (3.1a) and (3.1b) as

$$S_L^>(\varepsilon) = w\sigma_L^>(\varepsilon),$$

with

$$\sigma_L^>(\varepsilon) = (2/3)\,(\delta/(1+\delta))\,(\varepsilon - 1)^{3/2}, \quad (3.5a)$$

for $\varepsilon \geq 1$, and

$$S_L^<(\varepsilon) = w\sigma_L^<(\varepsilon),$$

with

$$\sigma_L^<(\varepsilon) = (2/3)\,(\delta/(1+\delta))\,(1 - \varepsilon)^{3/2} \quad (3.5b)$$

for $\varepsilon \leq 1$. Fig. 3 shows graphs of the action functions $\sigma^>$, $\sigma^<$, $\sigma_L^>$, and $\sigma_L^<$ over the range $0.25 < \varepsilon < 2$.

For a model of linear crossing potentials, the transition probabilities are expressed through the Airy function.[21] If these probabilities are normalized (N) to their values at $\varepsilon = 1$ (which allows one to disregard the coupling matrix element and provides enough information for calculating the tunneling correction factors, see Sec. IV), one has

$$P_{\mathrm{NAi}}(\varepsilon)|_{\varepsilon<1,\varepsilon>1} = N\mathrm{Ai}^2\left(\frac{1-\varepsilon}{\varepsilon_L}\right), \quad (3.6)$$

where

$$\varepsilon_L = ((1+\delta)/w\delta)^{2/3} \quad (3.7)$$

and $N = \mathrm{Ai}^{-2}(0) = 7.93$. Note that the argument of the Airy function in Eq. (3.6) can be written as $[(1-\varepsilon)/\varepsilon_L]_{\varepsilon\leq 1} = \left(3S_L^<(\varepsilon)/2\right)^{2/3}$ or $[(1-\varepsilon)/\varepsilon_L]_{\varepsilon\geq 1} = -\left(3S_L^>(\varepsilon)/2\right)^{2/3}$.

The extension of Eq. (3.6) to nonlinear potentials can be done in different ways. In what follows, we use the generalized Airy approximation which is appropriate for a description of thermally averaged underbarrier (tunneling) nonadiabatic

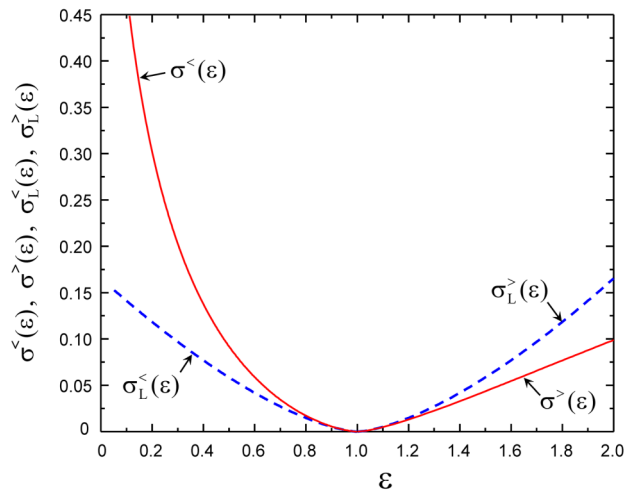


FIG. 3. *Ab initio* actions $\sigma^>$, $\sigma^<$, $\sigma_L^>$, and $\sigma_L^<$ vs the scaled energy $\varepsilon = E/E_a$.

transitions ($\varepsilon \le 1$) and overbarrier transitions ($\varepsilon \ge 1$) at not too high values of $\varepsilon$. For underbarrier transitions, expression (3.6) (valid for $\varepsilon$ not too much below the crossing-point energy) can be extended by smoothly replacing the action integral $S_L^<(\varepsilon)$ in the tunneling asymptotics $P_{\rm NAi}(\varepsilon)|_{\varepsilon<1, S_L^<>>1} \propto \exp[-2S_L^<(\varepsilon)]$ by its general counterpart $S^<(\varepsilon)$. Such a smooth replacement is possible here since the difference $S^<(\varepsilon) - S_L^<(\varepsilon)$ (when $\varepsilon$ approaches the crossing threshold $\varepsilon = 1$) decreases much more quickly than $S_L^<(\varepsilon)$ (see Fig. 3). Then, the NGAi approximation for the probabilities $P_{\rm NGAi}(\varepsilon)|_{\varepsilon\le1}$ assumes the form

$$P_{\rm NGAi}(\varepsilon)|_{\varepsilon\le1} = N\exp[-2S^<(\varepsilon) + 2S_L^<(\varepsilon)]{\rm Ai}^2\left(\frac{1-\varepsilon}{\varepsilon_{\rm L}}\right). \tag{3.8}$$

For overbarrier transitions, the expression in Eq. (3.6), in principle, should be modified to describe slower Stueckelberg oscillations of the probabilities for nonlinear potentials than for linear ones. However, if $P_{\rm NGAi}(\varepsilon)|_{\varepsilon\ge1}$ is used in thermal averaging over a small effective energy range $\delta\varepsilon$ above the threshold $\varepsilon = 1$, one can still keep an approximation $P_{\rm NGAi}(\varepsilon)|_{\varepsilon\ge1} \approx P_{\rm NAi}(\varepsilon)|_{\varepsilon\ge1}$. Indeed, the first Stueckelberg maximum of $P_{\rm NGAi}(\varepsilon)|_{\varepsilon\ge1}$ occurs at $\varepsilon \approx 1 - \varepsilon_L$. Across the energy range $\delta\varepsilon \approx \varepsilon_L$, the Boltzmann factor drops by $\exp[-\varepsilon_L(E_a/k_{\rm B}T)]$. For $T < 1000$ K, $E_a/k_{\rm B} = 5250$ K, and $\varepsilon_L \approx 0.45$, as estimated from Eq. (3.7) with $w \approx 10.3$ and $\delta \approx 1/3$, this drop amounts to more than one order of magnitude. Within the same energy range, before reaching their maximum, the probabilities increase by a factor of two. We, therefore, conclude that the approximation $P_{\rm NGAi}(\varepsilon)|_{\varepsilon\ge1} \approx P_{\rm GAi}(\varepsilon)|_{\varepsilon\ge1}$, which correctly describes the increasing part of the first Stueckelberg oscillation in the linear range of the potentials, can be accepted for thermal averaging. In this way, we write

$$P_{\rm NGAi}(\varepsilon)|_{\varepsilon\ge1} = N{\rm Ai}^2\left(\frac{1-\varepsilon}{\varepsilon_{\rm L}}\right). \tag{3.9}$$

Asymptotically, for $S^< >> 1$, $P_{\rm NGAi}$ in Eq. (3.8) approaches the NLL expression

$$P_{\rm NGAi}(\varepsilon)|_{\varepsilon<1, S^<>>1} = P_{\rm NLL}(\varepsilon) = \frac{N}{4\pi}\sqrt{\frac{\varepsilon_L}{1-\varepsilon}}\exp\left(-2S^<(\varepsilon)\right). \tag{3.10a}$$

Similarly, for $S_L^> >> 1$, $P_{\rm NGAi}$ in Eq. (3.9) approaches the NLZ expression

$$P_{\rm NGAi}(\varepsilon)|_{\varepsilon>1, S_L^>>1} = P_{\rm NLZ}(\varepsilon) = \frac{N}{\pi}\sqrt{\frac{\varepsilon_L}{\varepsilon-1}}\sin^2(S_L^>(\varepsilon) + \pi/4). \tag{3.10b}$$

This expression describes neither the first Stueckelberg oscillation (because of the restrictive condition $S_L^>(\varepsilon) >> 1$) nor the oscillatory pattern of supernumerary oscillations (because $S_L^>(\varepsilon)$ incorrectly substitutes $S^>(\varepsilon)$) and, therefore, it is not used in the calculation of thermally averaged probabilities. Nonetheless, a simplified version of Eq. (3.10b) is used as a normalization quantity in calculating the tunneling correction factors in Sec. IV. In this approximation (called here LZ classical, LZCl), the oscillating factor in Eq. (3.10b) is replaced by its mean value 1/2 (thus, the difference between $S_L^>(\varepsilon)$ and $S^>(\varepsilon)$ disappears) and the energy range is extended down to its lowest classically allowed limit $\varepsilon = 1$. The explicit expression for $P_{\rm NLZCl}(\varepsilon)$ is

$$P_{\rm NLZCl}(\varepsilon) = \frac{N}{2\pi}\sqrt{\frac{\varepsilon_L}{\varepsilon-1}}\Theta(\varepsilon-1), \tag{3.11}$$

where $\Theta(\varepsilon - 1)$ is the step function. The artificial divergence in Eq. (3.11) (at $\varepsilon \to 1$) is often considered unimportant when $P_{\rm LZCl}(\varepsilon)$ is used in averaging over $\varepsilon$ since the integral over $\varepsilon$ converges. At least, this is a standard approximation in the semiclassical LZ theory (see Sec. IV).

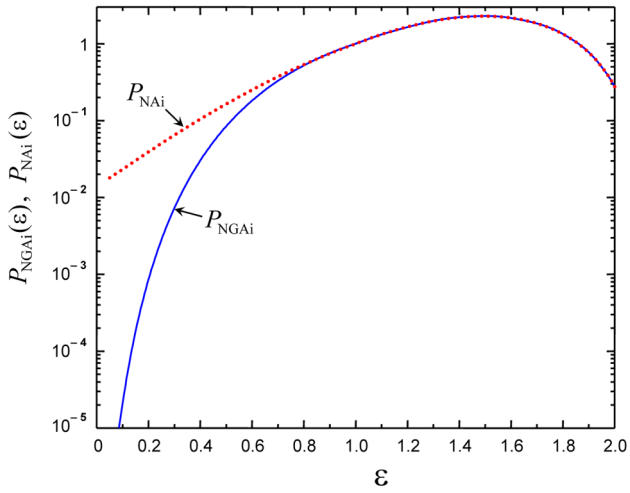


FIG. 4. Normalized generalized Airy ($P_{\rm NGAi}(\varepsilon)$) and Airy ($P_{\rm NAi}(\varepsilon)$) transition probabilities vs the scaled energy $\varepsilon = E/E_a$ over the range $0.05 < \varepsilon < 2$.

Fig. 4 presents normalized probabilities $P_{\rm NGAi}(\varepsilon)$ and $P_{\rm NAi}(\varepsilon)$. Within a certain energy range near $\varepsilon = 1$, the probabilities $P_{\rm NGAi}(\varepsilon)$ and $P_{\rm NAi}(\varepsilon)$ approach each other and demonstrate a smooth passage to Eq. (3.6). At the right of the energy range shown, the probabilities pass through their first Stueckelberg maxima. Note that for $\varepsilon < 1$, due to much stronger tunneling for linear potentials, $P_{\rm NAi}(\varepsilon)$ is notably larger than $P_{\rm NGAi}(\varepsilon)$.

## IV. AVERAGE QUANTUM CORRECTIONS TO THE LZ RATE COEFFICIENT

The relaxation rate coefficient $k_{10}(T)$, as calculated within the present reaction-coordinate approach, can be written as

$$k_{10}(T) = C(T) \cdot {}^{\rm LZCl}k_{10}(T), \tag{4.1}$$

where ${}^{\rm LZCl}k_{10}(T)$ is the rate coefficient calculated with LZCl nonadiabatic probabilities. The factor $C(T)$ takes into account the deviations from the LZCl approximation as described by the probabilities of Eqs. (3.8) and (3.9). It is expressed as the ratio of the thermally averaged transition probabilities $\bar{P}(T)$ and their $\bar{P}_{\rm LZCl}(T)$ counterparts. Within the GAi or NGAi nomenclature, the temperature dependence of the correction factor $C$ is more conveniently expressed through the dimensionless Arrhenius ratio $A = E_a/k_{\rm B}T$ such that

$$C_{\rm GAi}(A) = C_{\rm NGAi}(A) = \bar{P}_{\rm NGAi}(A)/\bar{P}_{\rm NLZCl}(A). \tag{4.2}$$

The expression for $\bar{P}_{\mathrm{NGAi}}(A)$, here, is given by

$$\bar{P}_{\mathrm{NGAi}}(A) = \int_0^\infty P_{\mathrm{NGAi}}(\varepsilon) \exp\left(-A(\varepsilon - 1)\right) A d\varepsilon, \qquad (4.3)$$

where $\varepsilon = 1$ (i.e., the energy $E_a$) is taken as the reference energy and the Boltzmann distribution function is normalized to unity across the energy range $1 \le \varepsilon < \infty$ (i.e., for $E > E_a$). A similar expression holds for $\bar{P}_{\mathrm{NLZCl}}(T)$ in which case it can be explicitly written as

$$\bar{P}_{\mathrm{NLZCl}}(A) = \frac{N}{2\pi}\sqrt{\pi A \varepsilon_L}. \qquad (4.4)$$

The accuracy of the reaction-coordinate approach depends on the character of convergence of the integral in Eq. (4.3) at its lower limit. Taken literally, the limit $\varepsilon = 0$ corresponds to asymptotically large values of $\zeta$ at the turning point, implying the breakdown of the reaction-coordinate approach. Therefore, the integral in Eq. (4.3) should be regarded as converged at such energies $\varepsilon$ for which the range of the reaction coordinate values is not too large. Representations of the integrand in Eq. (4.3) in the form of canonically weighted (CW) GAi probabilities $P^{\mathrm{CW}}_{\mathrm{NGAi}}(\varepsilon, A) = P_{\mathrm{NGAi}}(\varepsilon) \exp\left(A(1-\varepsilon)\right)$ are shown in Fig. 5 for selected values of the Arrhenius ratio $A$ across the range $0.05 < \varepsilon < 2$.

Here, all curves exhibit single-maximum behavior and cross at the point $\varepsilon = 1$ due to the normalization of the probabilities. The maximum for the curve with $A = 3$ corresponds to the first Stueckelberg oscillation of the probabilities (with its maximum near $\varepsilon = 1.5$), noticeably shifted to lower energies due to the interplay with the Boltzmann factor $\exp\left(A(1-\varepsilon)\right)$. For $A > 3$, the maxima arise from the interplay of the energy dependence of the probabilities at classically forbidden energies and the Boltzmann factor. For the deep tunneling region, with $S^<(\varepsilon) >> 1$, one can use the asymptotic expression for $P_{\mathrm{NGAi}}(\varepsilon)$, Eq. (3.10a), such that, for $A >> 1$, one has

$$P^{\mathrm{CW}}_{\mathrm{NGAi}}(\varepsilon, A) \approx P_{\mathrm{NLL}}(\varepsilon) \exp\left(A(1-\varepsilon)\right) = \frac{N}{4\pi}\sqrt{\frac{\varepsilon_L}{1-\varepsilon}} \exp\left(-2S^<(\varepsilon) + A(1-\varepsilon)\right). \qquad (4.5)$$

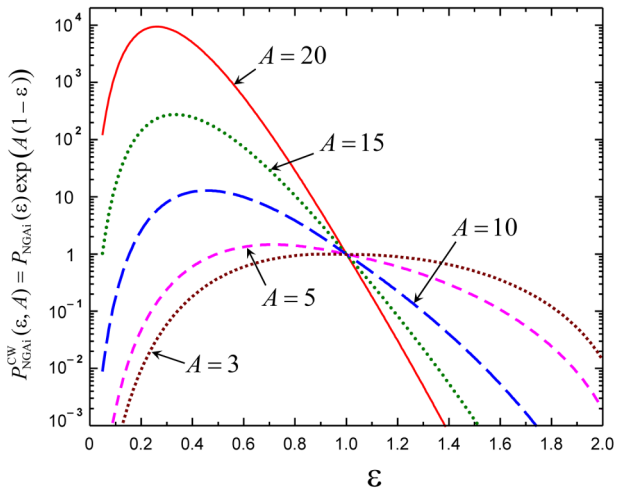


FIG. 5. Energy dependence of CW transition probabilities $P^{\mathrm{CW}}_{\mathrm{NGAi}}(\varepsilon, A) = P_{\mathrm{NGAi}}(\varepsilon)\exp(A(1-\varepsilon))$.

The given considerations have the following significance for the temperature dependence of $C_{\mathrm{GAi}}(A)$. For medium temperatures, characterized by not too large values of $A$, $C_{\mathrm{GAi}}$ will be close to unity, because the tunneling contribution to the integral for $\varepsilon < 1$ is only of little importance. For low temperatures, with $A >> 1$, $C_{\mathrm{GAi}}(A)$ will be much larger than unity due to tunneling. With decreasing energy in this temperature range, the decreasing tunneling probabilities and increasing Boltzmann factors lead to a maximum in $P^{\mathrm{CW}}_{\mathrm{NGAi}}(\varepsilon, A)$. This occurs at an energy $\varepsilon = \varepsilon^*(A)$, the vicinity of which contributes to $C_{\mathrm{GAi}}(A)$. As discussed in Ref. 17, $\varepsilon^*$ represents the energy of an optimal trajectory out of the Boltzmann ensemble of reaction coordinate trajectories. For sufficiently large $A$, the function $\varepsilon = \varepsilon^*(A)$ can be found from the maximum of the exponent in Eq. (4.5), i.e., from the equation

$$\frac{\partial}{\partial \varepsilon}\left(-2S^<(\varepsilon) + A(1-\varepsilon)\right)\Big|_{\varepsilon=\varepsilon^*(A)} = -\left(2\partial S^<(\varepsilon)/\partial\varepsilon + A\right)\Big|_{\varepsilon=\varepsilon^*(A)} = 0. \qquad (4.6)$$

Then, by using Eq. (4.5), one can estimate $C_{\mathrm{GAi}}(A)$ by the steepest descent (SD) approximation as $C_{\mathrm{GAi}} \approx C^{\mathrm{SD}}_{\mathrm{LL}}$ with

$$C^{\mathrm{SD}}_{\mathrm{LL}}(A) = \sqrt{\frac{A}{4(1-\varepsilon)\partial^2 S^<(\varepsilon)/\partial^2\varepsilon}} \times \exp\left(-2S^<(\varepsilon) + A(1-\varepsilon)\right)\Big|_{\varepsilon=\varepsilon^*(A)}. \qquad (4.7)$$

This expression coincides with Eq. (4.9) of Ref. 17 (used there for an exponential model of diabatic potentials), except for the pre-exponential factor (assumed there to be close to unity). The passage of the expression of Eq. (4.7) to its counterpart for the Airy transition probability is realized with decreasing $A$. Then, $\varepsilon^*$ moves up to unity, the exponent and the pre-exponential factors in Eq. (4.7) approach their limits appropriate for crossing linear potentials, and $C^{\mathrm{SD}}_{\mathrm{LL}}$ approaches the Airy function coefficient $C^{\mathrm{SD}}_{\mathrm{Ai}}(A)$.[17] A peculiar property of the Airy function approximation should be noted: the coefficient $C^{\mathrm{SD}}_{\mathrm{Ai}}(A)$ (which ignores the overbarrier transitions and describes the underbarrier transitions in the SD approximation) exactly coincides with the accurate Airy function coefficient $C_{\mathrm{Ai}}(A)$ (which accounts for the overbarrier and underbarrier transitions in the integral in Eq. (4.3)). This is due to the cancellation of errors which have been noted earlier in discussion of the Airy function approximation in a different context.[25] As a consequence, the expression for $C^{\mathrm{SD}}_{\mathrm{LL}}(A)$ in Eq. (4.7), which is strictly valid only for $A >> 1$, can be extrapolated to smaller values of $A$ such that, with a reasonable accuracy, it represents the correction factor $C_{\mathrm{GAi}}(A)$ across the whole range of $A$ of interest for tunneling corrections.

This observation is illustrated in Fig. 6 which shows plots of $C_{\mathrm{GAi}}(A)$ (red solid line) and $C^{\mathrm{SD}}_{\mathrm{LL}}(A)$ (open red circles). Also shown are the partial contributions to $C_{\mathrm{GAi}}(A)$ from the underbarrier contribution $C^-_{\mathrm{GAi}}(A)$ and the overbarrier contribution $C^+_{\mathrm{GAi}}(A)$ (blue dots) (see left ordinate axis). In addition, this figure shows the plot of the optimal energy $\varepsilon^* = \varepsilon^*(A)$ (green dashed line, see right ordinate axis), i.e., the energy of the optimal trajectory.

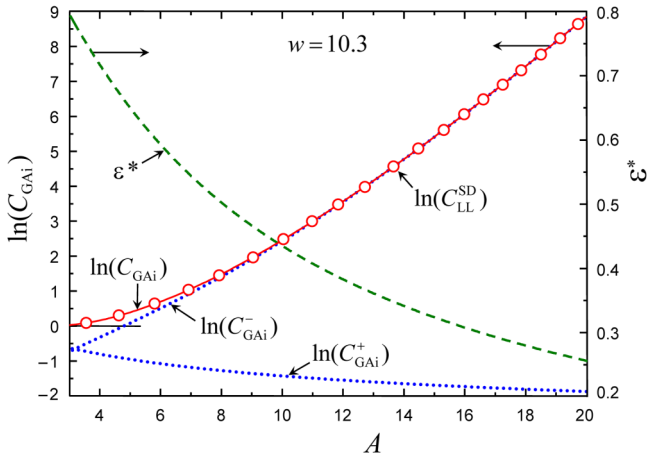


FIG. 6. Tunneling correction factors $C_{\mathrm{GAi}}(A)$, their partial contributions $C^{-}_{\mathrm{GAi}}(A)$ and $C^{+}_{\mathrm{GAi}}(A)$, and SD approximations to LL, $C^{\mathrm{SD}}_{\mathrm{LL}}(A)$ (left ordinate axis). Also shown is the plot of the optimal energy $\varepsilon^{*} = \varepsilon^{*}(A)$ (right ordinate axis).

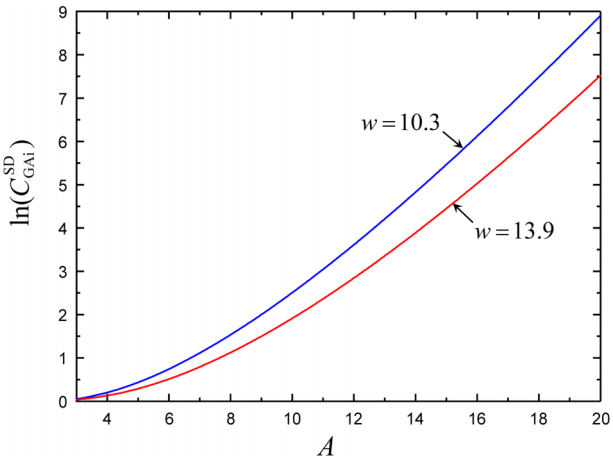


FIG. 7. Tunneling correction factors $C^{\mathrm{SD}}_{\mathrm{GAi}}(A)$ for the *ab initio* value $w = 10.3$ (blue line) and $w = 13.9$ (red line) from Eq. (3.2) (the latter value of $w$ is obtained from $w = 10.3$ replacing the effective mass $\mu^{*}$ by the reduced mass $\mu$).

Three features should be noted in particular.

(i) The underbarrier contribution to $C_{\mathrm{GAi}}(A)$, $C^{-}_{\mathrm{GAi}}(A)$, for $A > 3$, becomes larger than the overbarrier one, $C^{+}_{\mathrm{GAi}}(A)$. The decrease in the overbarrier contribution with increasing $A$ (i.e., with decreasing temperature) is a result of the progressively smaller relative contribution of the first Stueckelberg maximum of the GAi transition probability compared to the divergent LZCl contribution.

(ii) The steepest descent Landau-Lifshitz (SDLL) approach ($C^{\mathrm{SD}}_{\mathrm{LL}}(A)$ coefficient) provides an excellent approximation to the accurate GAi approach ($C_{\mathrm{GAi}}(A)$ coefficient) over the whole range of $A$ of interest for the tunneling effect.

(iii) The optimal energy $\varepsilon^{*} = \varepsilon^{*}(A)$ does not become too small even for large values of $A$. For instance, for $A = 17$ (i.e., at room temperatures), $\varepsilon^{*}$ is about 0.3. As seen from Fig. 2, for this energy, the range $\Delta z$ of $z$ that contributes to the probability is about 0.5 $a_0$. Since this value of $\Delta z$ is noticeably smaller that the characteristic range of the anisotropy $\Delta R = |dR_c(\theta)/d\theta|_{\theta=\theta_a}$ being about 1.3 $a_0$ in Table I, one would expect that the reaction coordinate approach, that requires the fulfillment of the condition $\Delta z/\Delta R << 1$, performs reasonably well. On the other hand, it is clear that for still higher values of $A$, this condition will not be satisfied, such that for ultra-low temperatures, the reaction coordinate approximation breaks down.

One can avoid solving Eq. (4.6) for $\varepsilon^{*}(A)$ by using a parametric representation of $C^{\mathrm{SD}}_{\mathrm{LL}}(A)$ from Eqs. (4.6) and (4.7) as

$$A(\varepsilon^{*}) = -2\partial S^{<}(\varepsilon^{*})/\partial\varepsilon^{*},$$
$$C^{\mathrm{SD}}_{\mathrm{LL}}(\varepsilon^{*}) = \sqrt{\frac{-\partial S^{<}(\varepsilon^{*})/\partial\varepsilon^{*}}{2(1-\varepsilon^{*})\partial^{2}S^{<}(\varepsilon^{*})/(\partial\varepsilon^{*})^{2}}} \times \exp\left(-2S^{<}(\varepsilon^{*}) - 2(1-\varepsilon^{*})\partial S^{<}(\varepsilon^{*})/\partial\varepsilon^{*}\right). \quad (4.8)$$

When the parameter $\varepsilon^{*}$ decreases from $\varepsilon = 1$ to a certain value $\varepsilon^{*} = \varepsilon_{\min}$ (with $\varepsilon_{\min}$ still satisfying the WKB criterion, Eq. (3.3)), $A$ increases from $A_{\min}$ to $A_{\max}$ and $C^{\mathrm{SD}}_{\mathrm{LL}}$ increases from near unity to a maximal value thus yielding the dependence of $C^{\mathrm{SD}}_{\mathrm{LL}}$ on $A$. The representation with Eqs. (4.7) and (4.8) allows one to recognize the dependence of the correction factor on parameters that enter into the action integrals. For instance, if the parameter $w$ increases (e.g., due to an increase in the effective mass) and $A$ is fixed, the correction factor $C^{\mathrm{SD}}_{\mathrm{LL}}$ decreases as the result of less pronounced tunneling. On the other hand, if the parameter $w$ increases and $T$ is fixed, $C^{\mathrm{SD}}_{\mathrm{LL}}$ may increase as the result of the interplay between the changes in $w$ and $A$. These two tendencies are illustrated by Fig. 7 and 8.

Fig. 7 shows plots of $C^{\mathrm{SD}}_{\mathrm{GAi}}$ vs $A$ for $E_a/k_{\mathrm{B}} = 5250$ K and two different values of $w$ which correspond to an effective mass $\mu^{*}$ ($w = 10.3$) and a reduced mass $\mu$ ($w = 13.9$) (an illustration of the effect of rotation of NO): here, the curve with larger $w$ lies below that with smaller $w$. Fig. 8 shows plots of $C^{\mathrm{SD}}_{\mathrm{GAi}}$ vs. $1/T$ for two values of $E_a/k_{\mathrm{B}} = 5250$ K and 4500 K ($w = 10.3$ and 9.5, respectively): here, the curve with larger $w$ lies above

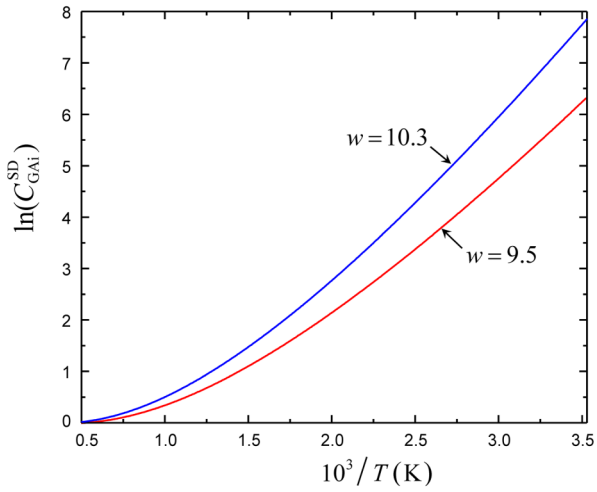


FIG. 8. Tunneling correction factors $C^{\mathrm{SD}}_{\mathrm{GAi}}(A)$ vs $1/T$ for the *ab initio* value $w = 10.3$ (blue line) (also shown is the plot of $C_{\mathrm{GAi}}$ with $w = 9.5$ which is obtained from $w = 10.3$ by lowering $E_a/k_{\mathrm{B}} = 5250$ K to $E_a/k_{\mathrm{B}} = 4500$ K, red line).

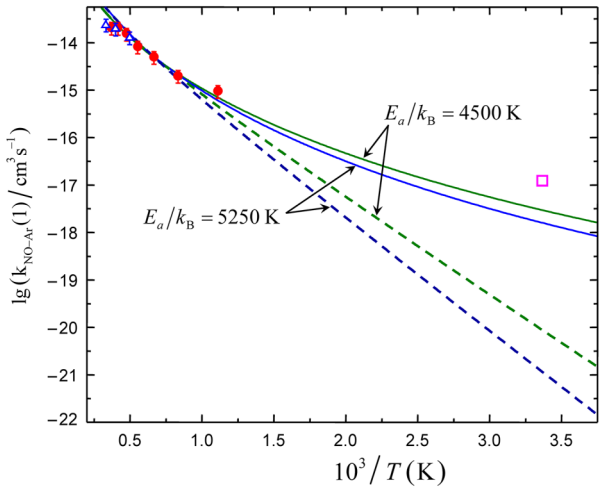


FIG. 9. Temperature dependence of the rate coefficients $C(T)\cdot{}^{LZ}k_{10}(T)$ (blue solid line) and ${}^{LZ}k_{10}(T)$ (blue dashed line) across 300–3000 K as fitted to the experimental high-temperature data and using the *ab initio* value $E_a/k_B = 5250$ K. Also shown are plots (green solid and dashed lines) with $E_a/k_B = 4500$ K as derived in Ref. 17 by parameter scaling; experimental data are shown by symbols: full red circles from Ref. 1, open blue triangles from Ref. 20, and open magenta square from Refs. 18 and 19.

that with smaller $w$ (an illustration of the effect of lowering the barrier). The counterintuitive conclusion that the lowering of the barrier decreases the tunneling correction is explained by the fact that the decrease is overcompensated by the increase of the Arrhenius factor in the full expression for the rate coefficient (see Fig. 9 in Sec. V).

## V. DISCUSSION

The rate coefficient calculated within the reaction coordinate approach and the LZCl approximation, ${}^{LZCl}k_{10}(T)$, assumes the form[17]

$$ {}^{LZ}k_{10}(T) = {}^{LZ}A T^{1/2}(T + T_{SO})\exp(-E_a/k_B T). \quad (5.1)$$

Here, the first factor ${}^{LZ}A$ includes parameters of the coupling and of the structure of the relevant crossing region, the second arises from the width of the trajectory manifold that crosses the dividing surface near the bottom of the potential and the crossing line at the energy $E_a$, the third is due to the Coriolis and the spin-orbit interaction, and the last factor accounts for the Boltzmann probability to reach the energy $E_a$. With $T_{SO}$ = 3225 K, the main contribution to the coupling is due to spin-orbit interaction, and deviations of ${}^{LZ}k_{10}(T)$ from a linear Arrhenius plot for $T < 2000$ K are hardly noticeable. Fig. 9 shows the corresponding plot of ${}^{LZ}k_{10}(T)$ (dashed blue line in Fig. 9) over the temperature range $300 < T < 2000$ K, drawn with the value of ${}^{LZ}A$ fitted such that the rate coefficient ${}^{LZ}k_{10}(T)$ assumes a value ${}^{LZ}k_{10}(T)|_{T=1500\ K} = 5\times10^{-15}$ cm$^3$ s$^{-1}$ which lies in the middle of the shock tube results (full red circles[1] and empty blue triangles[20]). Also shown are experimental results near 300 K by LIF and IR-UV double resonance techniques (empty magenta square[18,19]). The corrected rate coefficient of the present work, $C_{UAi}(T)^{LZ}k_{10}(T)$, with the correction factor taken from Fig. 8, is represented by a solid blue line. In order to illustrate the sensitivity of the rate coefficient to the main parameter of the interaction, i.e., the energy $E_a$, we also show rate coefficients with $E_a/k_B$ = 4500 K (dashed green line for the LZCl rate coefficient and solid green line for the GAi corrected LZ rate coefficient).

At high temperatures (near to 900 K, i.e., the lowest temperature of the shock tube experiments), one clearly observes the onset of contributions from tunneling which was analyzed in Ref. 17 within a semiempirical approach. Interestingly, the value of the effective mass suggested in Ref. 17 turned out to be close to that calculated in the present work using *ab initio* potentials. With decreasing temperature, the tunneling contribution increases and, at room temperature, the correction factor attains a value of about $10^4$. Still, the tunneling-corrected LZ rate coefficient is about a factor of 10 lower than the experimental result. This disagreement can have several reasons. First, the experimental results at $T$ = 300 K are open to criticism[9] and may represent an upper limit to the real rate coefficients. Second, assuming that the *ab initio* PESs are sufficiently accurate, the present theoretical treatment is still prone to uncertainties.

(i) As we have used two-dimensional potentials (in $R$ and θ) that describe the NO–Ar interaction for a fixed internuclear distance $r$ of NO (i.e., $r = r_e$), for the vibrational states $v = 0$ and $v = 1$ of the interacting NO–Ar pair, we have ignored corrections due to adiabatically averaged three-dimensional potentials (in $R$, θ, and $r$). We assume (see Sec. II) that this can only result in a few percent uncertainty of the energy $E_a$.

(ii) We have used the reaction-coordinate concept of tunneling, i.e., we have replaced the two-dimensional motion in $R$ and θ by a one-dimensional motion in the reaction coordinate $z$. We believe that this approximation is valid as long as the range $\delta z^*$ of $z$, which contributes significantly to the action integrals at the optimal energy $\varepsilon^*$, is noticeably smaller than the characteristic length $\delta R$ that characterizes the anisotropy of interaction. Taking $\delta z^*$ as a fraction of 1 a.u. (see Fig. 2) and identifying $\delta R$ with $dR_c/d\theta|_{\theta=\theta_a}$ from Table I, we conclude that the condition $\delta z^* << \delta R$ is indeed satisfied.

(iii) We have used the transition-state theory approach for the calculation of the LZCl rate coefficient and for the calculation of the tunneling correction factor, i.e., we relied on the assumption that a canonical distribution of rotational/translational modes of freely colliding species also becomes a canonical distribution over activated complex modes.

These simplifications would be avoided by using full three-dimensional PESs (i), a multi-dimensional description of tunneling (ii), and a complete dynamical description of the collision which relates thermal rate coefficients to state-specific cross sections (iii). Such extensions of the treatment appear beyond our present possibilities. Nevertheless, we believe that the present work provides a semi-quantitatively correct picture of tunneling and eliminates the large difference between the LZCl rate coefficients and the experimental results at room temperature.

## VI. CONCLUSIONS

We conclude this article by highlighting similarities and differences between the LT and LZ mechanisms of vibrational relaxation of diatomic molecules in collisions with nonreactive atoms under conditions when the interaction bears a purely repulsive character, and the coupling of the vibrational mode of the diatom to the translational-rotational modes of the colliding pair is weak. In our earlier study of the $N_2$ relaxation in He, we have extended the original, classical, LT theory (LTCl) to low temperatures by using the WKB approach (LTWKB).[13] At room temperature, the ratio ${}^{\mathrm{LTWKB}}k_{10}/{}^{\mathrm{LTCl}}k_{10}$ amounts to more than a factor of 100 and markedly increases for still lower temperatures. This is in agreement with experimental data available over wide temperature ranges (see Fig. 3 from Ref. 13). In the present work on NO relaxation in Ar, we have extended the LZCl theory to lower temperatures by using the WKB approach (LZWKB). At room temperature, here the ratio ${}^{\mathrm{LZWKB}}k_{10}/{}^{\mathrm{LZCl}}k_{10}$ amounts to a factor of $10^4$ and again further increases for still lower temperatures. This is in the direction of bringing theory into agreement with the limited available experimental data, though we have noted possible limitations of the present approach (see Sec. V).

In both cases (LT and LZ), the strong increase of the rate coefficients with decreasing temperature, as compared to extrapolated Landau-Teller and Arrhenius temperature dependences, is due to quantum effects. Within the WKB approximation, the latter can be treated by using information on the potentials in a quite narrow range of the reaction coordinate in the vicinity of the dividing surface. In both cases, the coupling of the rotation of the diatom to the diatom-atom motion can be expressed within an effective mass approximation. For $N_2$–He collisions, the effective mass was found to be about 10% smaller than the reduced mass $\mu$ of the collision pair, while for NO–Ar collisions, it amounts to 50%. This is due to the difference, for $N_2$–He and NO–Ar collisions, between the reduced mass of the collision pair $\mu$ and that of the diatom M ($\mu < M$ for $N_2$–He collisions and $\mu > M$ for NO–Ar collisions) and the difference of the anisotropy of the dividing surfaces (small anisotropy for $N_2$–He collisions and large anisotropy for NO–Ar collisions).

In summary, we conclude that the reaction-coordinate approximation applied to the NO + Ar relaxation within the WKB collision conditions accounts for the large quantum effects of the process. This result calls for more theoretical and experimental studies of this and the related processes at low temperatures. The case studied in this paper (NO + Ar collisions) represents an example where large tunneling corrections to the relaxation rate are expected. Other obvious candidates for a similar treatment are vibronic relaxations in collisions of open-shell species, e.g., in OH + raregas and $N_2$ + O collisions.

## ACKNOWLEDGMENTS

We most gratefully acknowledge the interest and the help of Millard Alexander who provided his code[22] for the NO–Ar *ab initio* potentials.

[1]K. Glänzer and J. Troe, J. Chem. Phys. **63**, 4352 (1975).
[2]R. P. Fernando and I. W. M. Smith, Chem. Phys. Lett. **66**, 218 (1979).
[3]E. S. Hwang, K. J. Castle, and J. A. Dodd, J. Geophys. Res. **108**, 1109 (2003).
[4]K. Glänzer and J. Troe, J. Chem. Phys. **65**, 4324 (1976).
[5]K. Glänzer and J. Troe, Ber. Bunsenges. Phys. Chem. **81**, 231 (1977).
[6]M. Quack and J. Troe, Ber. Bunsenges. Phys. Chem. **81**, 160 (1977).
[7]M. V. Ivanov, R. Schinke, and G. C. McBane, Mol. Phys. **105**, 1183 (2007).
[8]L. Doyenette and M. Margottin-Maclou, J. Chem. Phys. **84**, 6668 (1986).
[9]G. Hancock, M. Morrison, and M. Saunders, Phys. Chem. Chem. Phys. **11**, 8507 (2009).
[10]P. Pajón-Suárez, J. Rubayo-Soneira, and R. Hernández-Lamoneda, J. Phys. Chem. A **115**, 2892 (2011).
[11]L. Landau and E. Teller, Phys. Z. Sowjetunion **10**, 34 (1936).
[12]E. E. Nikitin, *Theory of Elementary Atomic and Molecular Processes in Gases* (Clarendon Press, Oxford, 1974).
[13]E. I. Dashevskaya, I. Litvin, E. E. Nikitin, and J. Troe, J. Chem. Phys. **125**, 154315 (2006).
[14]E. E. Nikitin, Mol. Phys. **7**, 389 (1964).
[15]E. E. Nikitin and S. Ya. Umansky, Faraday Discuss. Chem. Soc. **53**, 7 (1972).
[16]E. A. Andreev, S. Ya. Umansky, and A. A. Zembekov, Chem. Phys. Lett. **18**, 567 (1973).
[17]E. I. Dashevskaya, E. E. Nikitin, and J. Troe, Phys. Chem. Chem. Phys. **17**(1), 151 (2015).
[18]J. C. Stephenson, J. Chem. Phys. **59**, 1523 (1973).
[19]J. Kosanetzky, U. List, W. Urban, H. Vormann, and E. H. Fink, Chem. Phys. **50**, 361 (1980).
[20]K. Glänzer, Chem. Phys. **22**, 367 (1977).
[21]L. D. Landau and E. M. Lifshitz, *Quantum Mechanics* (Pergamon Press, Oxford, 1977), Sec. 51.
[22]M. H. Alexander, J. Chem. Phys. **111**, 7426 (1999).
[23]Y. Karni and E. E. Nikitin, Chem. Phys. **191**, 235 (1995).
[24]M. H. Alexander, P. Soldan, T. G. Wright, Y. Kim, H. Meyer, P. J. Dagdigian, and E. P. F. Lee, J. Chem. Phys. **114**, 5588 (2001).
[25]E. E. Nikitin, C. Noda, and R. N. Zare, J. Chem. Phys. **98**, 46 (1993).